PFC/JA-84-9

LIMITER HARD X-RAY EMISSION STUDIES DURING LOWER HYBRID CURRENT DRIVE EXPERIMENTS ON THE ALCATOR C TOKAMAK

D. S. Pappas, S. C. Texter, R. F. Gandy,
B. Lloyd, M. Porkolab, and
Alcator Group

April 1984

This work was supported by the U.S. Department of Energy Contract No. DE-AC02-78ET51013. Reproduction, translation, publication, use and disposal, in whole or in part by or for the United States government is permitted.

LIMITER HARD X-RAY EMISSION STUDIES DURING LOWER HYBRID CURRENT DRIVE EXPERIMENTS ON THE ALCATOR C TOKAMAK

D. S. Pappas, S. C. Texter, R. F. Gandy,
B. Lloyd, M. Porkolab, and
Alcator Group

ABSTRACT

Measurements of flux and energy spectra of the thick target bremsstrahlung produced by relativistic electrons colliding with the Alcator C limiters during lower hybrid current drive experiments are described. The qualitative behavior of the flux and energy spectra are in agreement with theoretical expectations with regard to the launched power spectrum and loop voltage programming. Additionally, a mechanism appears to exist which causes a transfer of parallel electron energy into perpendicular energy at the rf turn-off.

1. INTRODUCTION

During the early operation of tokamaks, runaway phenomena were a dominant feature of the discharges and hence a great deal of activity was directed toward studies of limiter hard x-ray emissions [1-7].

In the case of Alcator A, with the advent of good vacuum procedures, discharge cleaning and pulsed gas injection, runaway phenomena became less prominent [8]. Similar behavior occurred in Alcator C, where after six months of operation and with fine tuning of the pulsed gas fueling system, very low levels of hard x-ray emission and photoneutron emission were observed due to the low levels of runaway electrons impacting upon the plasma limiter [9]. More recently during lower hybrid current drive experiments on Alcator C, large increases in the limiter hard x-ray emission was observed at low densities ($\bar{n}_e < 5 \times 10^{13} cm^{-3}$) and at low energies ($E_{photon} < .5$ MeV) thus providing the motivation for these studies. Similar effects were also seen on PLT [10] and FT [11] during lower hybrid experiments and studies of those limiter emissions have led to a further understanding of lower hybrid wave-plasma interactions. More detailed understanding of lower hybrid effects on the plasma have been obtained from measurements of plasma bremsstrahlung on Alcator C [12,13] and PLT [10] where estimates as to the shape of the electron energy distributions were also deduced.

In this report we devote our attention to a study of the effects on relativistic electrons during lower hybrid current drive experiments in Alcator C by measuring the properties of hard x-ray emission arising from the molybdenum limiters. The temporal behavior of hard x-ray flux and energy spectra in the range 0.2 MeV $\leq E_{photon} \leq$ 2.0 MeV in both forward

and perpendicular (to B_T) directions are presented. Strong effects on these emissions have been observed in hydrogen with toroidal magnetic fields in the range 8 T $\leq$ B_T $\leq$ 10 T, plasma currents $I_p \approx 200$ kA and electron densities, $2 \times 10^{13} cm^{-3} \leq \bar{n} \leq 1 \times 10^{14} cm^{-3}$. The injected lower hybrid power during these experiments was in the range 600 kW $\leq P_{rf} \leq$ 900 kW.

2. EXPERIMENTAL DESCRIPTION

2.1 Alcator C Geometry and Hard X-ray Spectrometers

Figure 1 shows a schematic top view of Alcator C. The major and minor radii of the device are 64 cm and 16.5 cm respectively. Two 4 × 4 waveguide grills are located on opposite sides of the device, each fed by a 1 MW rf power system operating at 4.6 GHz [14]. Two pairs of poloidal limiters, each displaced 60° from the nearest waveguide array, are constructed from blocks of molybdenum each attached to a stainless steel ring. Two 2" × 2" NaI(Tℓ) scintillators coupled to photomultiplier assemblies are placed for forward (downstream of electron drift) and perpendicular viewing (right angles with respect to the electron drift) of limiter hard x-ray emission arising from the limiter pair located in the left portion of the torus (see Fig. 1). Each of the spectrometers is housed in a five inch lead collimator and is located in the equatorial plane of the device. The spectrometers are used to measure the temporal behavior of the flux and energy spectra of the thick target bremsstrahlung produced by high energy electron impact upon the above described limiter pair. Significant amounts of copper and stainless steel are contained in the toroidal magnet structure (25 cm and 10 cm in the forward and perpendicular directions respectively) which block the view between the limiters

and the hard x-ray detectors. The result is that the hard x-ray flux in the forward direction is attenuated by several orders of magnitude more than the flux in the perpendicular direction. For this reason in this report comparisons of the forward and perpendicular flux (at a given energy) are made only in a qualitative manner.

2.2 Alcator C Rf Power Spectrum

Figure 2 shows the Brambilla power spectra at 4.6 GHz launched by one of the 4 × 4 Alcator C waveguide grills for adjacent waveguides phased at 67.5°, 90° and 180° respectively [14]. Illustrated below the power spectra are the corresponding energies for relativistic electrons in Landau resonance with the launched waves. For current drive experiments, adjacent waveguides are normally phased at 67.5° or 90° in order to produce a travelling wave spectrum with ~ 2/3 of the power in the electron drift direction. In this case it is seen from Fig. 2 that most of the rf power in the electron drift direction lies between $n_\parallel = 1$ and $n_\parallel = 3$. For very low values of $n_\parallel$ close to 1 the slow wave mode converts to a fast wave and cannot access the plasma center. In Fig. 3, contours showing where this mode conversion occurs are indicated by the dotted curves [15]. The figure shows that waves having $n_\parallel$ as low as 1.2 (for $B_T = 10$ T and $\bar{n}_e \approx 3 \times 10^{13} cm^{-3}$) are accessible to most of the plasma volume. One can thus deduce from the above two figures that the range of affected electrons during the lower hybrid injection should be between 30 keV and 400 keV. In the following section we will see results consistent with this expectation.

3. RESULTS

3.1 Hard X-Ray Flux and Spectra from Discharges Without Lower Hybrid Injection

In the absence of rf power oscillograms of the electron density, the plasma current, and the perpendicular and forward hard x-ray emissions are shown in Fig. 4a. The time scale is 100 ms/division. At approximately 150 ms into the discharge the primary OH transformer is open circuited and the plasma current is allowed to decay with an L/R time of ~ 130 ms. During the current decay the line averaged density decays from $6 \times 10^{13} cm^{-3}$ to $1 \times 10^{13} cm^{-3}$. Both the perpendicular and forward hard x-ray flux slowly increase early in the discharge and then slowly decay in about 100 ms. The total flux as registered by each of the detectors is about equal but due to the stronger attenuation in the forward direction than in the perpendicular direction (more toroidal magnet winding material) the forward flux, if corrected for the attenuation, would greatly exceed that in the perpendicular direction. In Fig. 4b we show the forward and the perpendicular spectra in three distinct 100 ms time domains which are delineated in Fig. 4a (regions I, II and III). Since the "raw" spectra which we show in this report do not take into account the energy dependent attenuation due to the toroidal magnet winding, x-ray slope temperatures should not be inferred.

3.2 Measurements of Flux and Spectra with RF Injection with a Relative Waveguide Phasing of + 90°

In Fig. 5 we show an oscillogram of the traces of interest for a discharge with lower hybrid injection. Note on the plasma current trace

that dI/dt is nearly zero at about seventy-five milliseconds after the current has been allowed to inductively decay. As can be seen in the figure the flat-topping of the current coincides with the rf injection from the two waveguide arrays.

As can be seen in the figure the 60 GHz radiometer emission strongly increases at the rf turn-on and is strongly correlated with the presence of the rf. At rf turn-off this emission initially decreases and then increases to an even higher level than that measured in the presence of rf power. While this behavior is typical for the low density discharges discussed in this paper (here $\bar{n} < 5 \times 10^{13} cm^{-3}$) it was not seen during discharges at higher density ($\bar{n}_e > 5 \times 10^{13} cm^{-3}$) [16].

Turning now to the limiter hard x-ray emissions we see that the perpendicular flux shows a similar behavior to the 60 GHz emission both during and after the rf. Comparing the forward and perpendicular flux after the rf pulse note that while the perpendicular emission increases, in contrast, the forward emission (generally) decreases with a post-rf burst which is smaller than the flat top steady emission.

To gain some insight into this behavior we have looked in more detail at the hard x-ray spectra for this same discharge. In Fig. 6 the energy spectra in both the forward and perpendicular directions were obtained in three regions of time (i.e., just before, during, and after the rf pulse). Looking first at the forward spectra, in region II we see photon events up to about 2 MeV. In region III (i.e., during the rf pulse and hence where $dI/dt \approx 0$ and V_{Loop} is very small) we see that the number of events in the low energy portion of the spectra ($E_{photon} < 0.5$ MeV) has increased and that the number of high energy events ($E_{photon} > 0.5$ MeV) has decreased.

These effects can be accounted for by (1) the resonance effect on the fast electrons caused by the launched waves (for $E_{photon} < 0.5$ MeV) and (2) since $V_{Loop} \approx 0$ the higher energy electron population decreases.

In region IV (i.e., just after the rf pulse) we observe that the low energy portion of the spectrum has fewer counts than the low energy spectrum in region III and that the number of counts in the high energy portion of the spectrum ($E_{photon} > 0.5$ MeV) has increased. These observations can be explained by the absense of launched lower hybrid waves and hence disappearance of any resonance wave-particle effects on the electrons (in the range of 30-400 keV as discussed in Section 2.2) and due to the increase of the loop voltage at rf turn-off. Since dI/dt and V_{Loop} are no longer small, once more electrons are accelerated to high energies by the dc electric field and photon events are registered for $E_{photon} >$ 0.5 MeV as in time domain II.

The interesting phenomenon to note from the perpendicular spectra is the increase in the tail population above ~ 1 MeV when the rf is turned off. This hardening of the spectrum in region IV over that in region III is possibly due to collisional isotropization. An alternate explanation is excitation of an instability which causes pitch angle scattering of particles from the forward direction into the perpendicular direction. Similar behavior to the above was observed for flat-topped (dI/dt = 0) discharges when $\Delta\phi = +67°$.

3.3 Measurement of Flux and Spectra for Rf Injection with Relative Waveguide Phasing of - 90°

The - 90° phasing case (i.e., the bulk of the rf power now launched in the opposite direction to the ohmic electron drift) presents a somewhat interesting situation in that "flat-topping" of the plasma current is not attainable and the loop voltage is not reduced to zero. The traces of interest are shown in Fig. 7. Note that $V_L \neq 0$, $dI/dt \neq 0$ and that as in the + 90° phasing case, the 60 GHz radiometer signal and hard x-ray emission increase at rf turn-on. In fact, this increase is even greater than in the + 90° case. This may be due to the fact that only about 70% of the total power in the Fourier spectrum can be launched in a given direction leaving roughly 30% to propagate in the opposite direction. This oppositely directed power can draw electrons to high energies via wave-particle interaction so that the loop voltage then has a very strong acceleration effect on these electrons. This enhanced limiter hard x-ray emission is corroborated by the observation of both harder plasma x-ray spectra and greater 60 GHz antenna radiation temperature for the $-\pi/2$ case over the $+\pi/2$ case [16].

Now looking at the forward and perpendicular limiter hard x-ray spectra, shown in Fig. 8 (where four 50 ms time gate periods are shown) the main feature to note is that during the rf pulse the high energy portions ($E_{photon} > 0.5$ MeV) of the forward spectra persists whereas in the + 90° phasing case the high energy events disappeared. This is expected since the loop voltage is not zero in this case so that the source of relativistic electrons is not extinguished. Also of interest is the strong enhancement of the high energy portion of the perpendicular

spectrum at rf turn-off (region IV) over the spectra taken during the rf pulse (region III) which (as in the + 90° and + 67° cases) is suggestive of a mechanism causing pitch angle scattering of high energy electrons into the perpendicular direction. Since the perpendicular collisional diffusion time is ~ 40 ms (100 keV electron), this process is too slow to alone explain the observed effects (i.e., the observed increase in the perpendicular flux at rf turn-off shown in Fig. 7 occurs on a much shorter time scale).

3.4 High Frequency Bursting Effects

In Fig. 9 are shown phenomena of interest in a case where $dI/dt \neq 0$ and thus the loop voltage is not zero. The relative waveguide phasing is + 67°. Looking at the limiter hard x-ray emission with an NaI detector viewing in the perpendicular direction we see some high frequency structure, both during and after the rf pulse. The high frequency phenomena after the rf pulse is not unusual and is typically accompanied by high frequency oscillations on the ω_{pe} emissions. The structure on the hard x-ray emissions during the rf injection however is unusual and may be related to the fact that after 30 ms of rf, an arc in one waveguide array caused that system to shut down for the rest of the discharge. The remaining rf power was insufficient to maintain a current flat top so that a loop voltage quickly developed. This loop voltage had a strong accelerating effect on the rf-formed high energy electron tail. This situation is similar to that which exists after the rf pulse. An expanded view of these oscillations is shown in Fig. 10 which clearly indicates their periodic nature. A similar behavior was observed in PLT [10]. The significance of these observations is that they suggest some regular

mechanism for pitch angle scattering of particles into the perpendicular direction. This may be caused by a wave-particle interaction (such as the anomalous Doppler effect [17] or to collisional isotropization. The critical velocity above which electrons are pitch angle scattered via the anomolous Doppler instability is given by: $v_{crit} = v_{th} (\omega_{ce}/\omega_{pe}) \lambda^{1/2}$ where $\lambda = \ln (\omega_{ce}^2/\omega_{pe}^2 \delta)$ and δ = tail-to-bulk electron density ratio [17]. For Alcator type conditions (B = 10 T, $n_e = 5 \times 10^{13} cm^{-3}$, T_e = 2 keV, $\delta \sim 10^{-3}$), the critical energy is: $E_{crit} \approx 1/2\ m\ v_{crit}^2 \sim 400$ keV. This corroborates the fact that only after rf shutoff do we see significant x-ray emission above ~ 500 keV (due to an induced E-field) and thus meet the criterion for this instability. These types of discharges will be further studied in the next series of lower hybrid experiments on Alcator C.

REFERENCES

[1] Gorbunov, E. P., Dolgov-Savel'ev, G. G., Mukhovatov, V.S., Strelkov, V. S., Yavlinskii, N. A., Sov. Phys.-Tech. Phys. 5 (1961) 1089: Investigation of a Toroidal Discharge in a Strong Magnetic Field; Mateev, V. V., Sokol'ov, A. D., ibid, 1084: Hard X-Ray Radiation from Tokamak-2, A Toroidal System.

[2] Matveev, V. V., Sokol'ov, A. D. Suchkova, L. A, Sov. Phys.-Tech. Phys. 8 (1961) 530: Investigation of Hard X-Ray Radiation from a Plasma in a Strong Magnetic Field.

[3] Artsimovich, L. A., Nucl. Fus. 12 (1972) 215: Tokamak Devices.

[4] Knoepfel, H., Zweben, S. J., Oak Ridge National Laboratory Report ORNL/TM-6103 (1977): Dynamics of High Energy Runaway Electrons in the Oak Ridge Tokamak.

[5] Von Goeler, S., Stodiek, W., in Controlled Fusion and Plasma Physics Research (Proc. 5th Eur. Conf. Grenoble) 1 (1972) 2: High Energy Electrons in ST Tokamak Discharges.

[6] Von Goeler, S., Stodiek, W. Sauthoff, N., Selberg, H., in Proc. of the 3rd Int. Symp. on Toroidal Plasma Confinement, Germany, 1973, Max-Planck-Institut fur Plasmaphysik, Garching, Germany (1973): X-Ray Spectra in the ST Tokamak.

[7] Knoepfel, H., Spong, D. A., Nucl. Fus. 19 (1979) 785: Review paper, Runaway Electrons in Toroidal Discharges.

[8] Boxman, G., Coppi, B., Dekock, L., Meddens, B., Oomens, A., Ornstein, L., Pappas, D., Parker, R., Pieroni, L., Segre, S., Schuller, F., Taylor, R., Proc. of the 7th Eur. Conf. on Plasma Physics, Lausanne, Switzerland, 1975: Low and High Density Operation of Alcator.

[9] Pappas, D. S., Furnstahl, R. J., Kochanski, G. P., Wysocki, F. J., Nucl. Fusion 23 (1983) 1285: Studies of Neutron Emission During the Start-Up Phase of the Alcator C Tokamak.

[10] Von Goeler, S., Stevens, J., Karney, C., Barnabei, S., Bitter, M., Chu, T., Efthimion, P., Hill, K., Hooke, W., Jobes, F., Mazzucato, E., Meservey, E., Motley, R., Roney, P., Sauthoff, N., Sesnik, S., Taylor, G., Tenney, F., Valeo, E., Princeton Plasma Physics Laboratory Report 2012 and in Proc. 5th Topical Conf. on Rf Plasma Heating, February 1983, Madison, Wisconsin, p. 96.

[11] Santini, F., Barbato, E., DeMarco, F., Podda, S., Tucillo, A., Phys. Rev. Lett., Vol. 52, No. 15, 1984, p. 1300, Anomalous Doppler Resonance of Relativistic Electrons with Lower Hybrid Waves Launched in the Frascati Tokamak.

[12] S. C. Texter, B. Lloyd, M. Porkolab, J. Schuss, Bull. Am. Phys. Soc. 28, 1162 (1983), Plasma X-ray Emission in the 20-500 keV Range During Lower Hybrid Current Drive on Alcator.

[13] Porkolab, M., Lloyd, B., Schuss, J., Takase, Y., Texter, S., Watterson, R., Bonoli, P., Englade, R., Fiore, C., Gandy, R., Granetz, R., Greenwald, M., Swinn, D., Lipschultz, B., Marmar, E., McCool, S., Pappas, D., Parker, R., Pribyl, P., Rice, T., Terry, J., Wolfe, S., Proc 4th Intl. Symp. on Rf Heating, Rome, Italy, March 1984; Lower Hybrid Experiments at the 1 MW Level on Alcator C: Heating and Current Drive.

[14] Porkolab, M., Schuss, J. J., Lloyd, B., Taskase, Y., Texter, S., Watterson, R., Bonoli, P., Englade, R., Fiore, C., Gandy, R., Granetz, R., Greenwald, M., Gwinn, D., Lipschultz, B., Marmar, E., McCool, S., Pappas, D., Parker, R., Pribyl, P., Rice, J., Terry,

J., Wolfe, S., MIT Plasma Fusion Center Report 83-6 and in Proc. 5th Topical Conf. on Rf Plasma Heating, February 1983, Madison, Wisconsin: Lower Hybrid Current Drive and Heating Experiments up to the 1 MW Level in Alcator C.

[15] Lloyd, B., Schuss, J. J., Bull. Am. Phys. Soc. 28 No. 8, October 1983, 2111: Ray Tracing and Accessibility Calculations in the Lower Hybrid Regime.

[16] Gandy, R. F., Yates, D. H., Lloyd, B., Porkolab, M., Schuss, J., Bull. Am. Phys. Soc. 28, 1162 (1983) Electron Plasma Frequency Emission During Current Drive on Alcator C.

[17] Parail, V. V., Potgutse, O. P., Sov. J. Plasma Phys., Vol 2, No. 2, March 1976, 125: Instability of the Runaway-Electron Beam in a Tokamak.

FIGURE CAPTIONS

FIGURE 1 Schematic top view of Alcator C showing relative positions of rf waveguide grills, limiters, and hard x-ray spectrometers.

FIGURE 2 Contours of accessibility for waves having $n_\parallel = 1.1$ and $n_\parallel = 1.2$ with $B_T = 10$ T, $\bar{n}_e = 3 \times 10^{13} cm^{-3}$ and $T_{eo} = 2$ keV.

FIGURE 3 Brambilla power spectrum of the Alcator C 16 waveguide grill at 4.6 GHz.

FIGURE 4 (a) Oscillogram of traces of interest for typical 8 T hydrogen discharge with no rf injection.

(b) Forward and perpendicular limiter hard x-ray spectra in three distinct 100 msec time domains.

FIGURE 5 Oscillogram of the traces of interest for a discharge with rf injection with relative waveguide phasing of +90°.

FIGURE 6 Forward and perpendicular limiter hard x-ray spectra in three regions of time (i.e., just before, during, and after the rf pulse) for the discharge shown in Fig. 5.

FIGURE 7 Oscillogram of the traces of interest for a discharge with rf injection with relative waveguide phasing of -90°.

FIGURE 8 Forward and perpendicular limiter hard x-ray spectra in four regions of time for the discharge of Fig. 7.

FIGURE 9 Traces of interest for a discharge with rf injection with relative waveguide phasing of +67°. High frequency structure appears on the limiter hard x-ray emissions during and after the rf probe.

FIGURE 10 Expanded view of the limiter emissions for the discharge shown in Fig. 9 indicating their periodic nature.

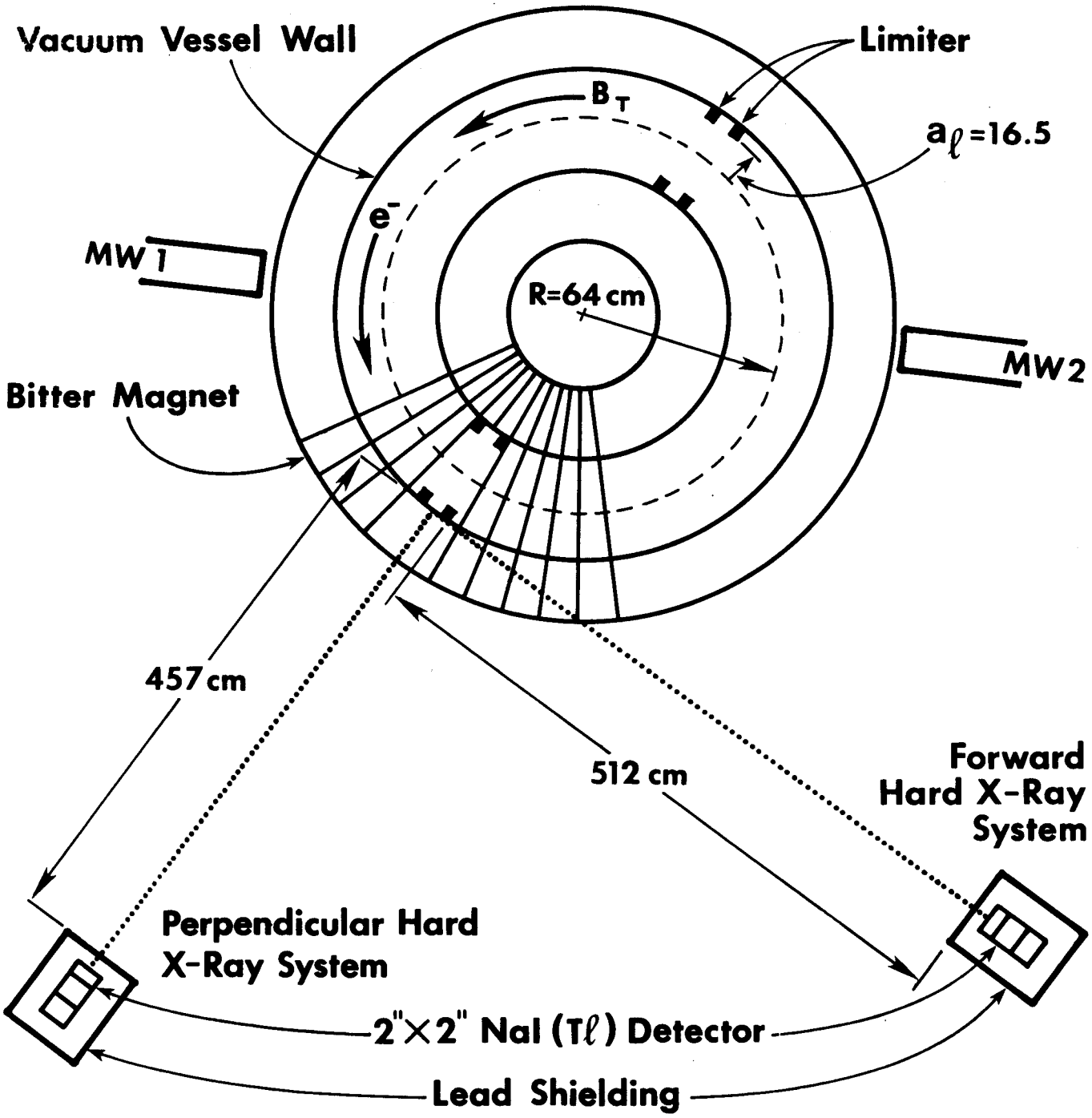
Vacuum Vessel Wall
Limiter
B_T
a_ℓ=16.5
e^-
MW 1
R=64 cm
MW 2
Bitter Magnet
457 cm
512 cm
Forward
Hard X-Ray
System
Perpendicular Hard
X-Ray System
2"×2" NaI (Tℓ) Detector
Lead Shielding

FIGURE 1

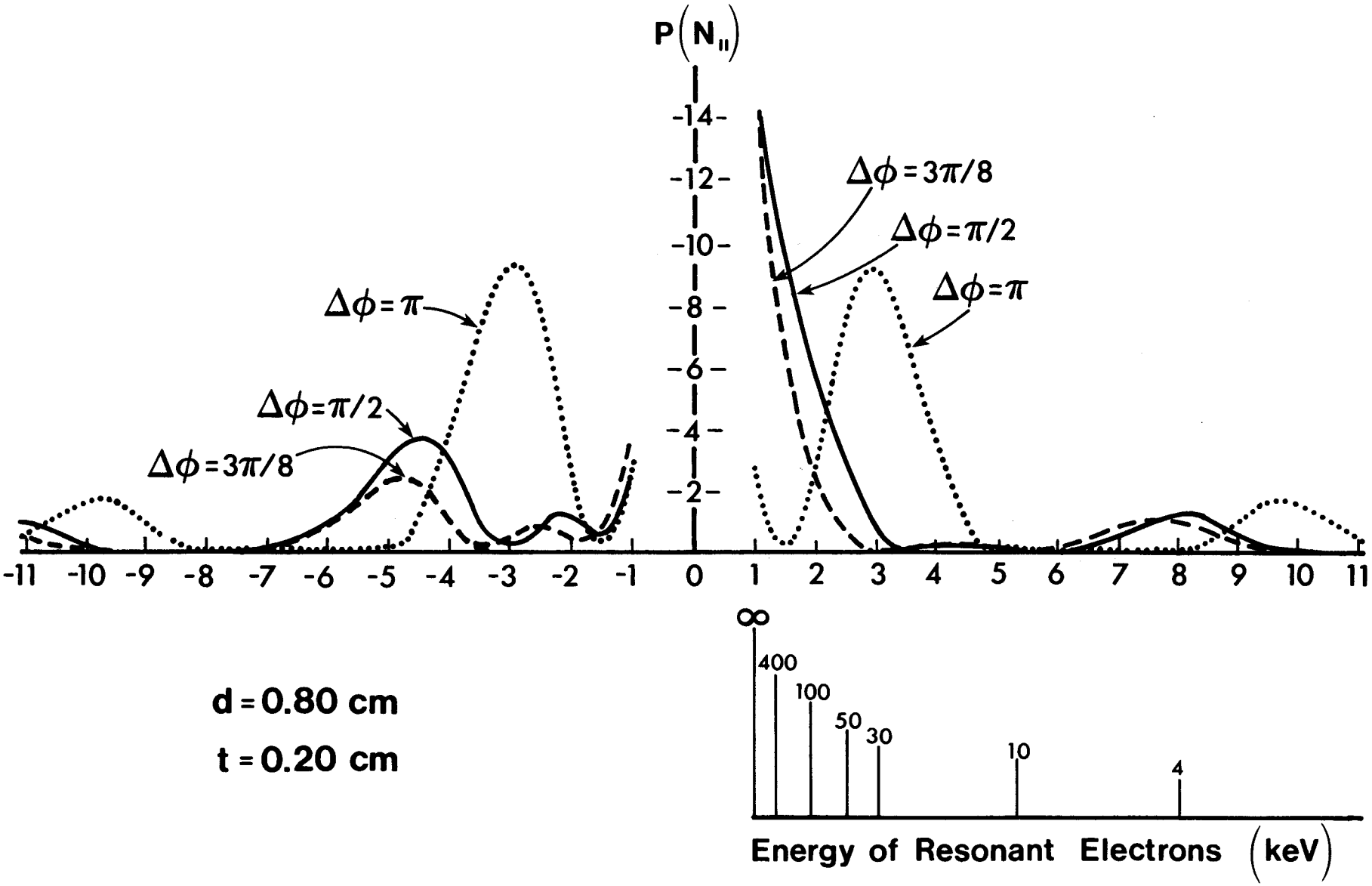
P(N∥)
-14-
-12-
-10-
-8-
-6-
-4-
-2-
Δφ=3π/8
Δφ=π/2
Δφ=π
Δφ=π
Δφ=π/2
Δφ=3π/8
-11 -10 -9 -8 -7 -6 -5 -4 -3 -2 -1 0 1 2 3 4 5 6 7 8 9 10 11
d = 0.80 cm
t = 0.20 cm
∞
400
100
50
30
10
4
Energy of Resonant Electrons (keV)

FIGURE 2

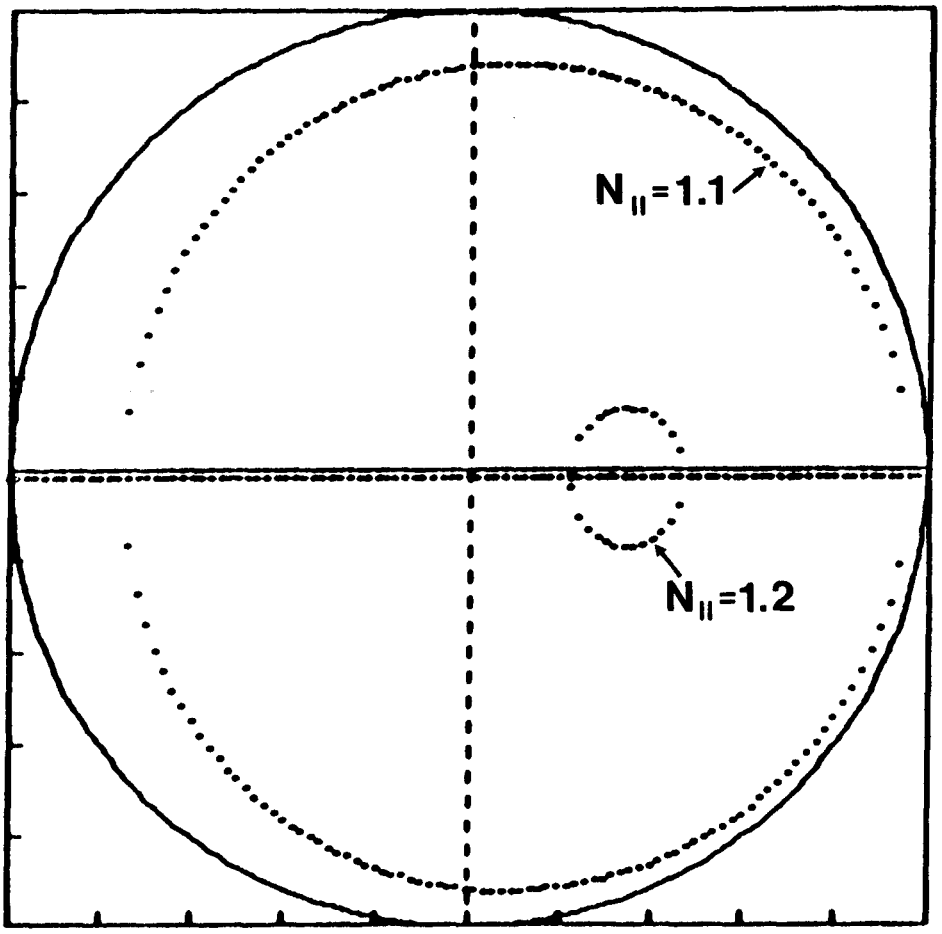

FIGURE 3

Limiter Hard X-Ray Pulse Height Spectra Without RF

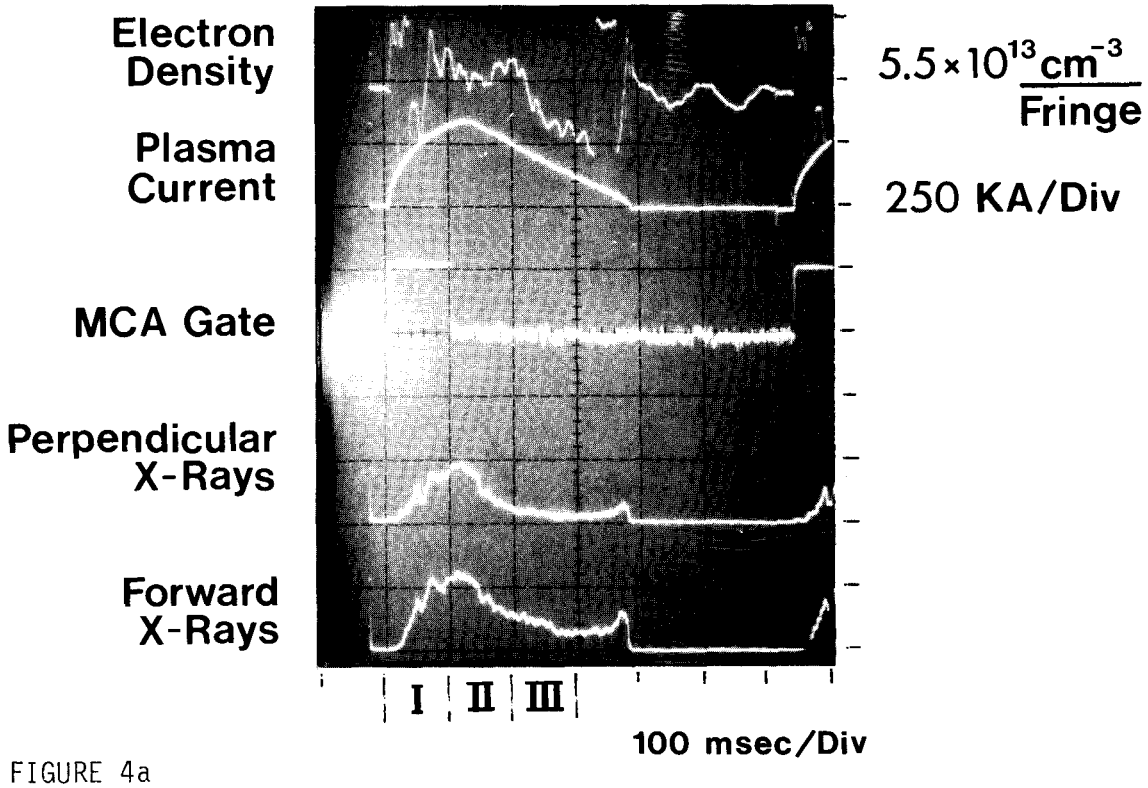

FIGURE 4a

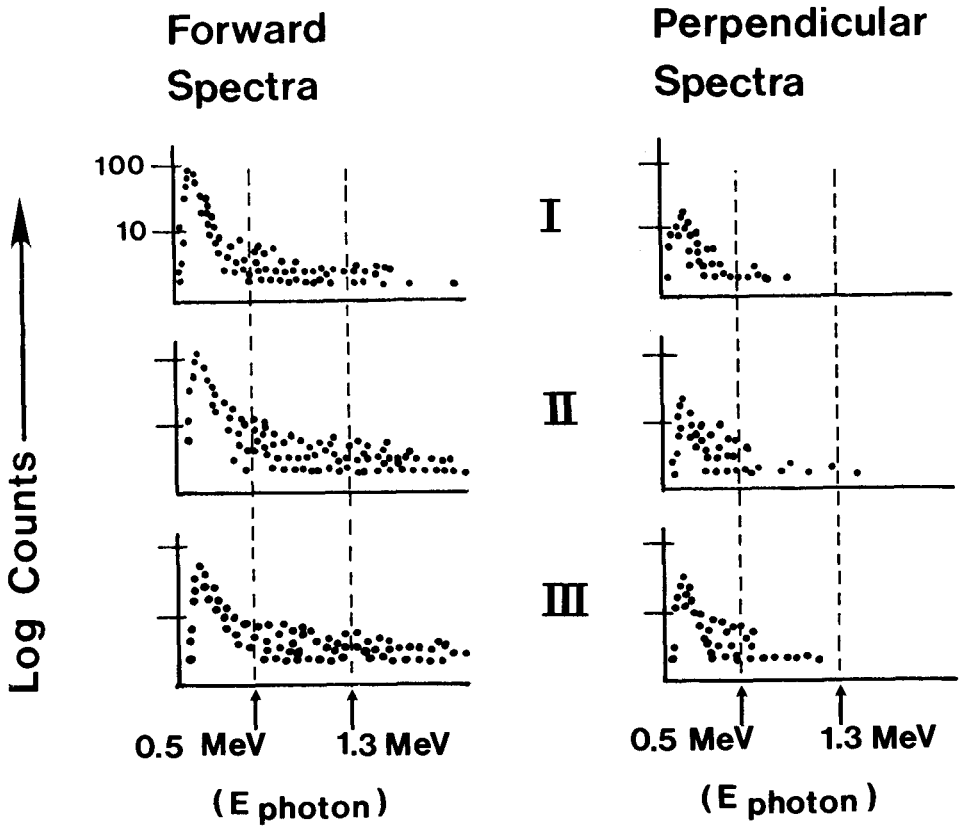

FIGURE 4b

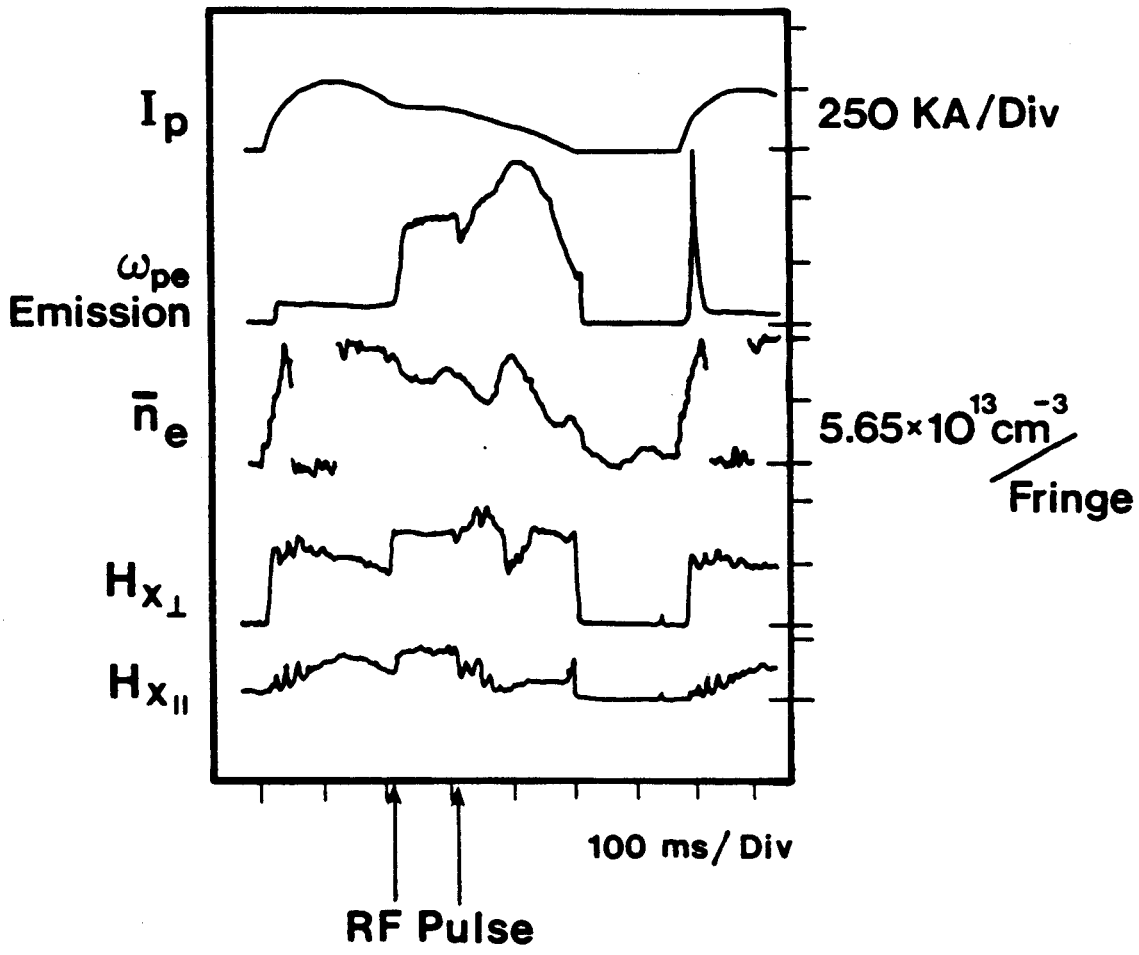
I_p
250 KA/Div
ω_{pe}
Emission
$\bar{n}_e$
$5.65\times10^{13}cm^{-3}$
Fringe
$H_{x_\perp}$
$H_{x_{||}}$
100 ms/ Div
RF Pulse

FIGURE 5

LIMITER HARD X-RAY PULSE HEIGHT SPECTRA WITH RF

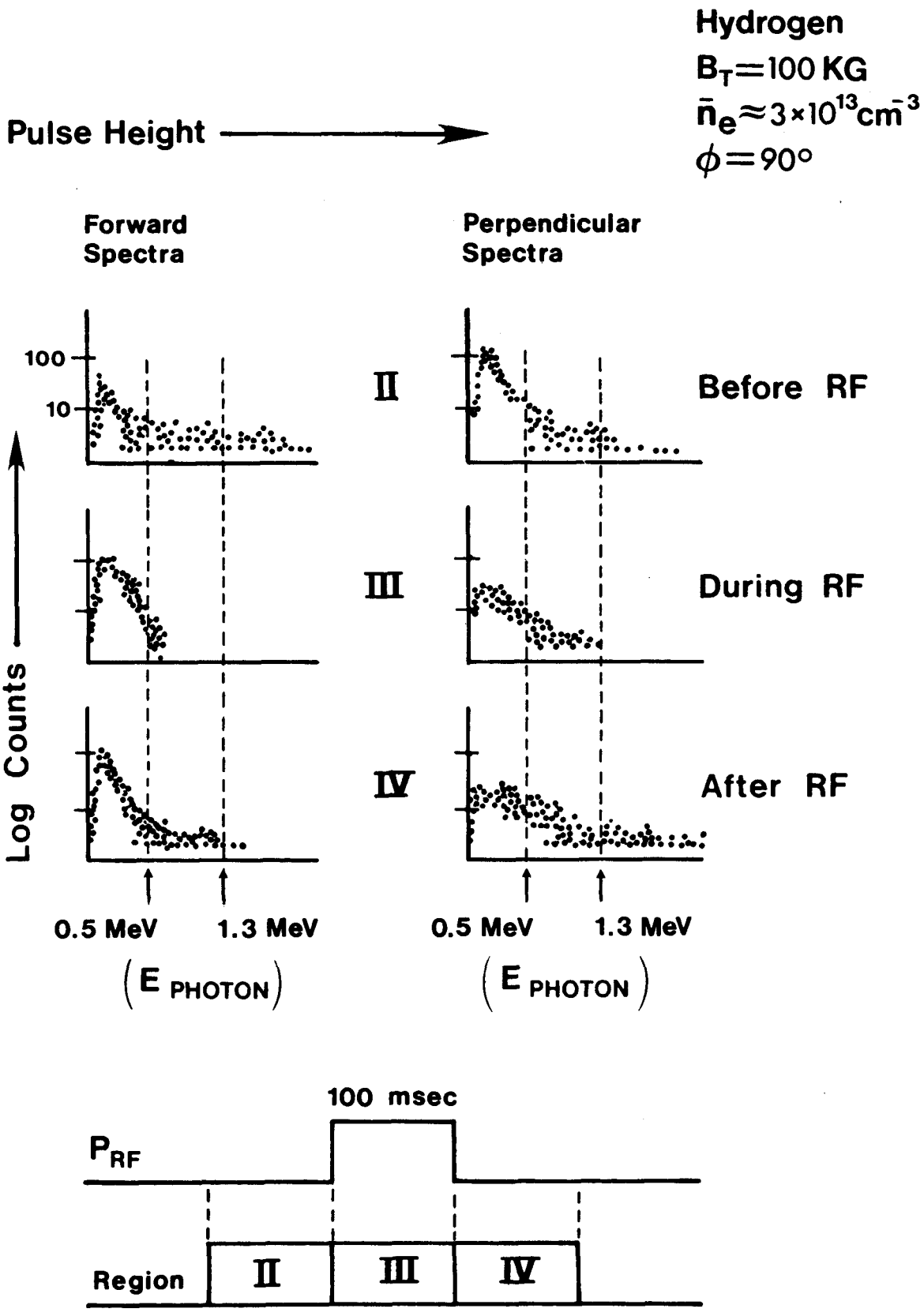

FIGURE 6

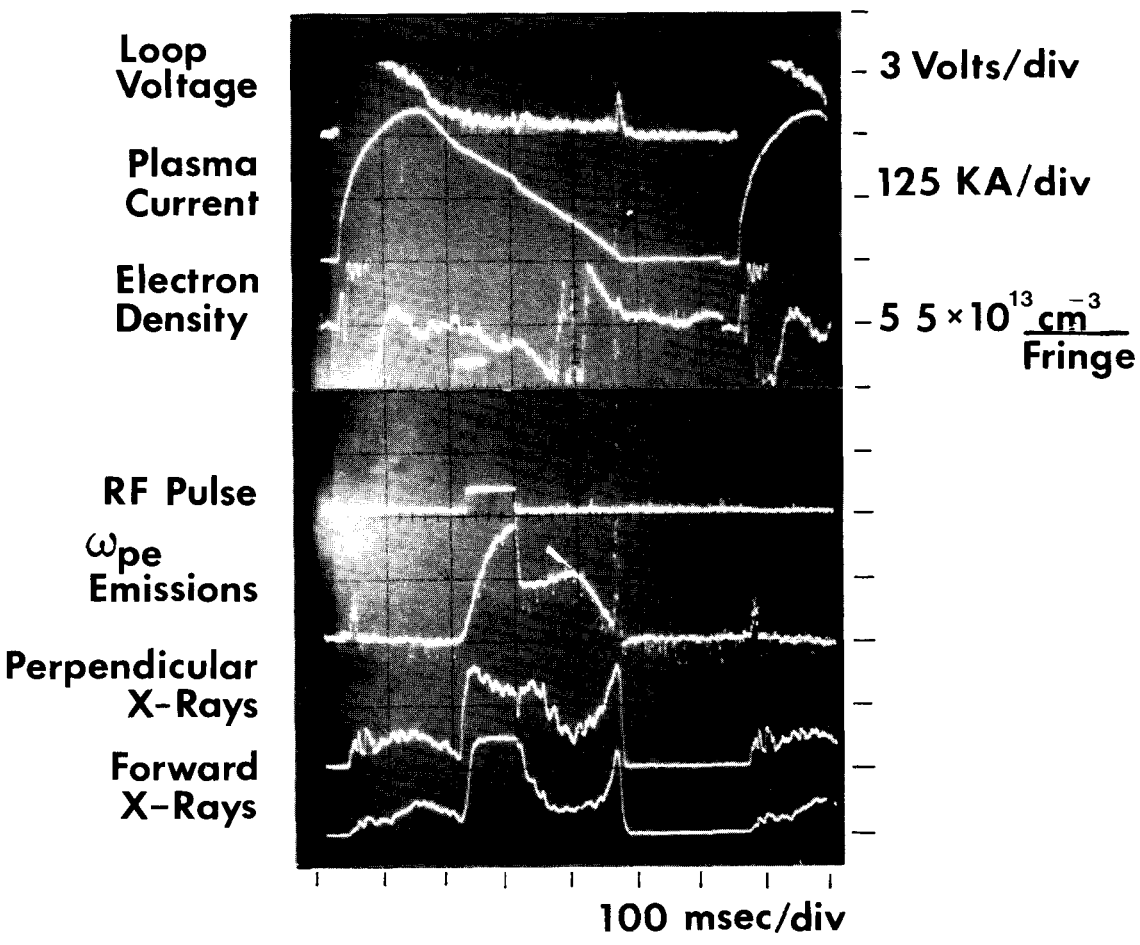
Hydrogen
B_T = 100 KG
ϕ = -90°
Loop Voltage
Plasma Current
Electron Density
RF Pulse
ω_{pe} Emissions
Perpendicular X-Rays
Forward X-Rays
3 Volts/div
125 KA/div
5 5 × 10^{13} cm^{-3} / Fringe
100 msec/div

FIGURE 7

LIMITER HARD X-RAY PULSE HEIGHT SPECTRA WITH RF

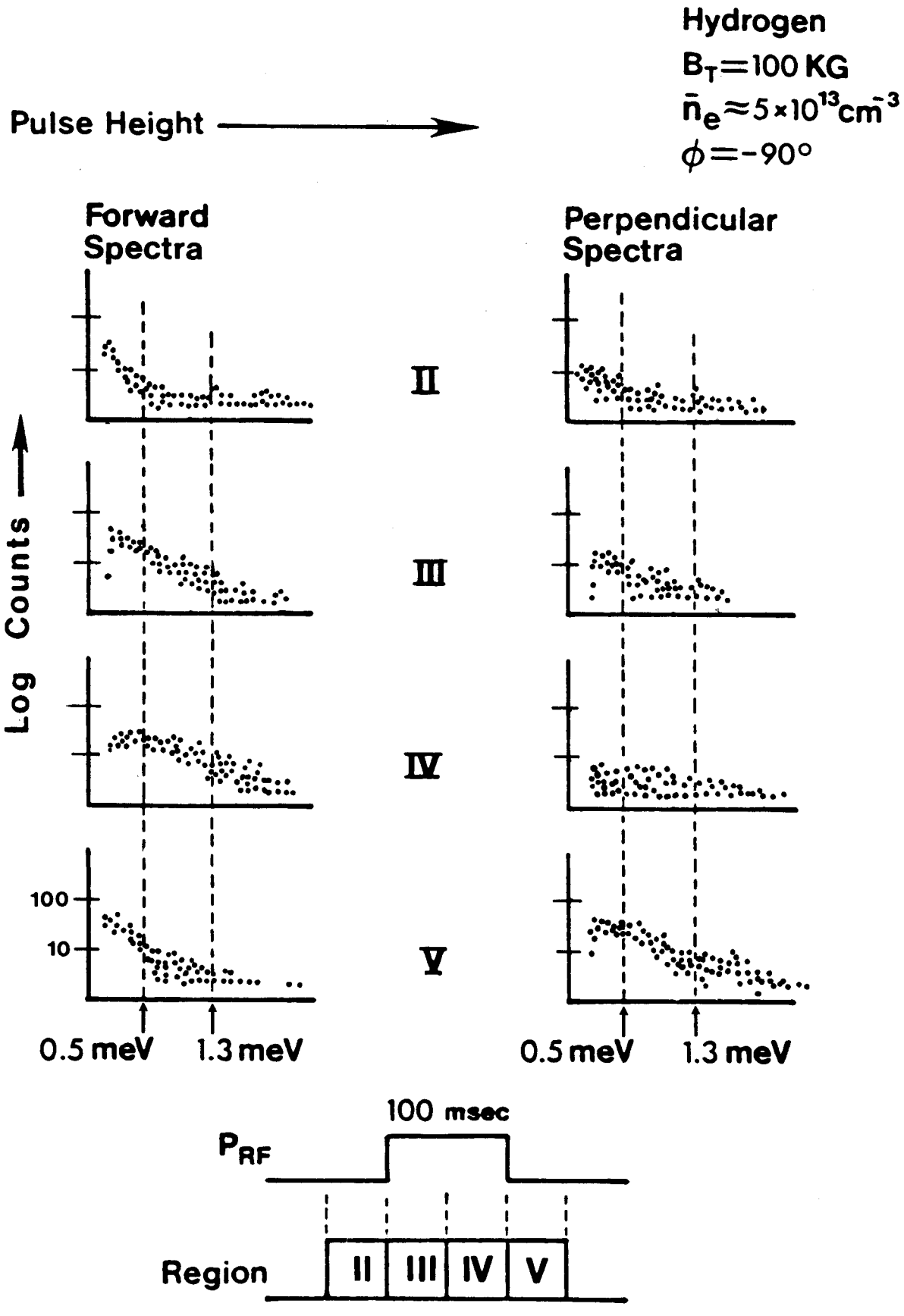

FIGURE 8

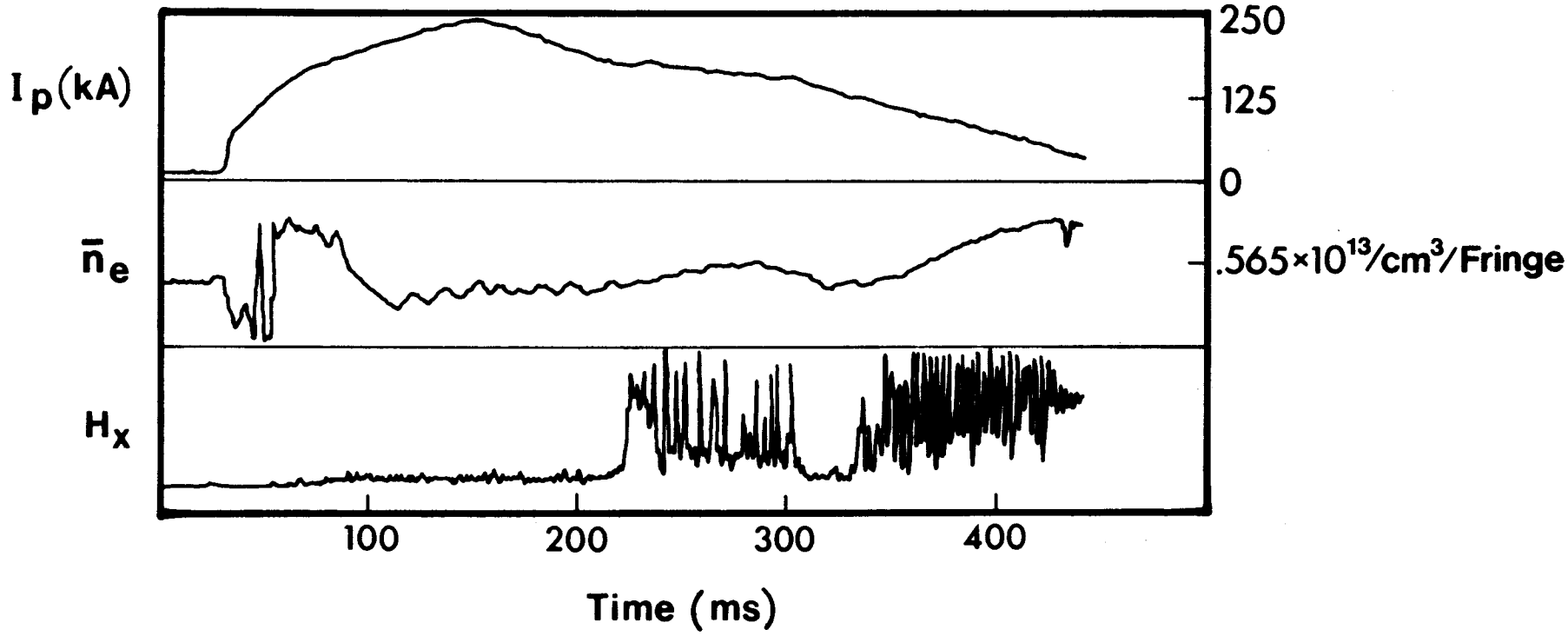
I_p(kA)
250
125
0
$\bar{n}_e$
.565×10^{13}/cm^3/Fringe
H_x
100
200
300
400
Time (ms)

FIGURE 9

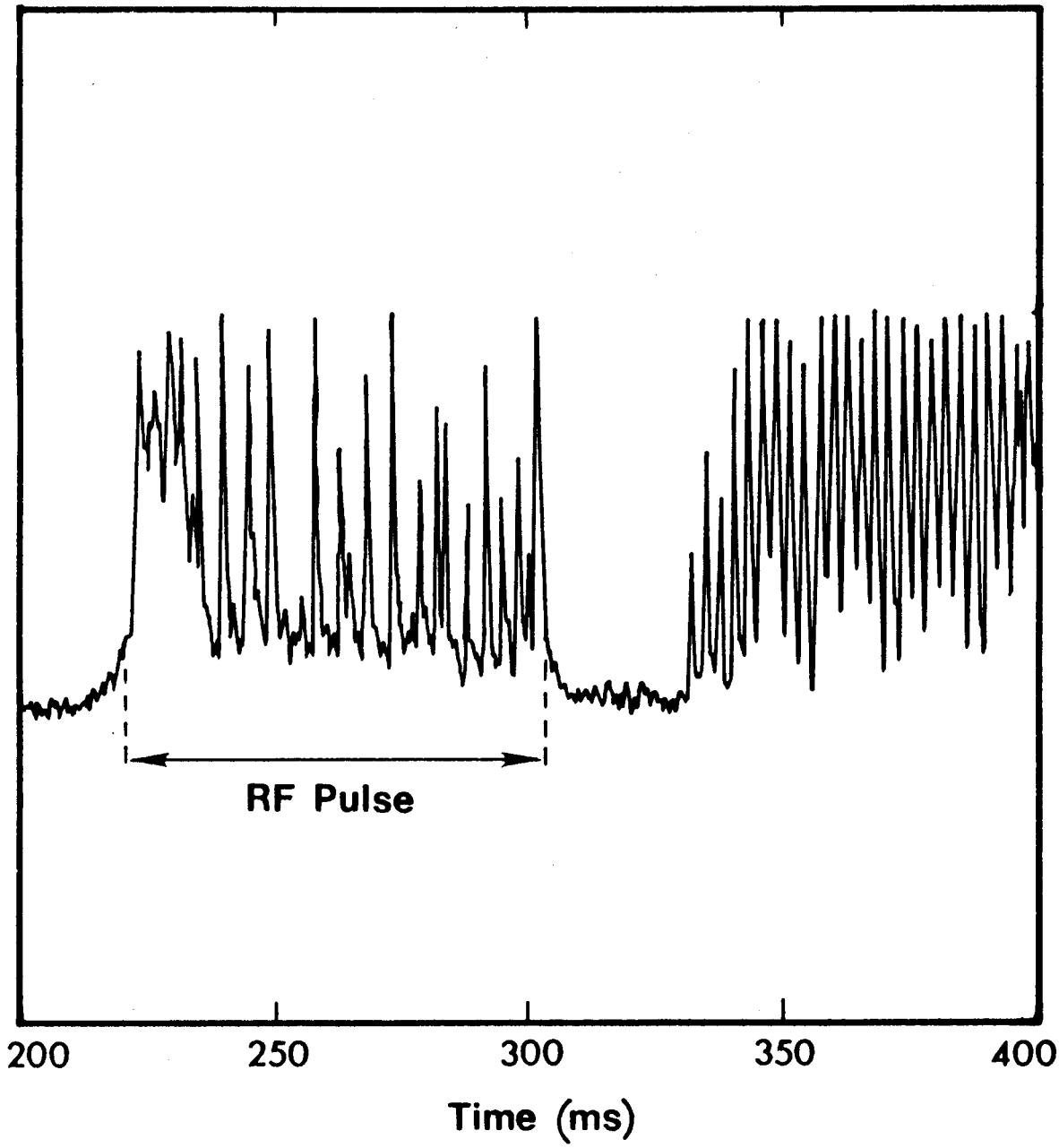

FIGURE 10